Title: Large-scale Gradient Dysfunction of the Functional Connectome in Major Depression

Author affiliations: Mingrui Xia[1,2,3], Jin Liu[1,2,3], Xiaoyi Sun[1,2,3], Qing Ma[1,2,3], Xiaoqin Wang[4,5], Dongtao Wei[4,5], Yuan Chen[6], Bangshan Liu[7,8], Chu-Chung Huang[9], Yanting Zheng[10], Yankun Wu[11], Taolin Chen[12], Yuqi Cheng[13], Xiufeng Xu[13], Qiyong Gong[12], Tianmei Si[11], Shijun Qiu[10], Ching-Po Lin[14,15], Jingliang Cheng[6], Yanqing Tang[16], Fei Wang[16], Jiang Qiu[4,5], Peng Xie[17,18,19], Lingjiang Li[7,8], Yong He[1,2,3*] and DIDA-Major Depressive Disorder Working Group

[1] State Key Laboratory of Cognitive Neuroscience and Learning, Beijing Normal University, Beijing, 100875, China
[2] Beijing Key Laboratory of Brain Imaging and Connectomics, Beijing Normal University, Beijing, 100875, China
[3] IDG/McGovern Institute for Brain Research, Beijing Normal University, Beijing, 100875, China
[4] Key Laboratory of Cognition and Personality (SWU), Ministry of Education, Chongqing, 400715, China
[5] Department of Psychology, Southwest University, Chongqing, 400715, China
[6] Department of Magnetic Resonance, The First Affiliated Hospital of Zhengzhou University, Zhengzhou, 450052, China
[7] Department of Psychiatry, The Second Xiangya Hospital, Central South University, Changsha, Hunan 410011, China
[8] Mental Health Institute of Central South University, China National Clinical Research Center on Mental Disorders (Xiangya), China National Technology Institute on Mental Disorders, Hunan Technology Institute of Psychiatry, Hunan Key Laboratory of Psychiatry and Mental Health, Changsha, Hunan 410011, China
[9] Institute of Cognitive Neuroscience, School of Psychology and Cognitive Science, East China Normal University, Shanghai 200062, China.
[10] Department of Radiology, The First Affiliated Hospital of Guangzhou University of Chinese Medicine, Guangzhou 510405, China
[11] Peking University the Sixth Hospital (Institute of Mental Health), National Clinical Research Center for Mental Disorders & Key Laboratory of Mental Health, Ministry of Health (Peking University), Beijing, 100191, China
[12] Huaxi MR Research Center (HMRRC), Department of Radiology, West China Hospital, Sichuan University, Chengdu, 610041, China
[13] Department of Psychiatry, First Affiliated Hospital of Kunming Medical University, Kunming, 650032, China
[14] Institute of Science and Technology for Brain-Inspired Intelligence, Fudan University, Shanghai, 200433, China
[15] Institute of Neuroscience, National Yang-Ming University, Taipei, 11221, China
[16] Department of Psychiatry, The First Affiliated Hospital of China Medical University, Shenyang, 110001, China
[17] Institute of Neuroscience, Chongqing Medical University, Chongqing, 400016, China
[18] Chongqing Key Laboratory of Neurobiology, Chongqing, 400016, China
[19] Department of Neurology, The First Affiliated Hospital of Chongqing Medical University, Chongqing, 400016, China

***Corresponding Author:** Yong He, PhD., State Key Laboratory of Cognitive Neuroscience and Learning, Beijing Key Laboratory of Brain Imaging and Connectomics, IDG/McGovern Institute for Brain Research, Beijing Normal University, Beijing, 100875, China. E-mail: yong.he@bnu.edu.cn.

Keywords: brain network, fMRI, functional connectivity, hierarchy, gene expression

Manuscript information: 19 text pages, 4 figures, 1 table.
(Supplementary Information: 6 figures, 8 tables.)

Abstract

Major depressive disorder (MDD) is associated with coexisting disturbances in low-level sensory processing and high-order cognitive functions. However, the neurobiological mechanism underlying these phenotype deficits remains poorly understood. Here, we collect large-sample, multisite resting-state functional magnetic resonance imaging data (1,150 patients with MDD and 1,084 healthy controls) and postmortem gene expression data. We show downgraded and contracted connectome gradients that are mainly involved in primary sensory and transmodal regions in patients with MDD relative to healthy controls, leveraging an association with gene expression enriched in transsynaptic signaling and calcium ion binding. Machine learning approaches based on support vector regression suggest that the alterations of connectome gradients in patients significantly predict depressive symptoms. These results shed light on gradient dysfunction of the large-scale functional connectomes in MDD and consolidate the spectrum deficits of sensory and cognitive processing in this disorder.

Introduction

Major depressive disorder (MDD) is one of the most common and globally burdening psychiatric disorders[1]. Neuropsychological studies suggest that patients with MDD present with deficits not only in low-level sensory processing but also in high-order cognitive functions such as self-awareness, rumination, working memory, executive control, and reward processing[2, 3, 4, 5]. Although many prior studies have reported widespread abnormalities in brain structure and function in MDD[6, 7, 8, 9, 10, 11], the neurobiological mechanism underlying the coexisting deficits in sensory and cognitive processing remains to be elucidated.

Hierarchical architecture is one of the fundamental organizational principles of the human brain, allowing for efficient encoding and integration of information communication from sensation to cognition[12]. Resting-state functional MRI (R-fMRI)[13] and the cutting-edge gradient decomposition framework[14] enable researchers to noninvasively investigate the hierarchical architecture of the macroscale functional connectome *in vivo*[14, 15]. In healthy adults, the network architecture of the macroscale connectome follows a principal gradient along the axis from the primary to the transmodal systems. Such a pattern provides insights into the brain basis of the spectrum of sensory input and cognitive processing[14] and is largely comparable to various cortical features, including microstructural myelination[16] and transcriptional profiles[17, 18]. Moreover, the connectome hierarchy is altered during development[19] and in brain disorders such as autism[20]. Regarding MDD, connectome dysfunction using R-fMRI has been frequently reported, involving the primary visual and sensorimotor systems[6, 21, 22, 23] and transmodal systems such as the default mode network (DMN) and frontoparietal network (FPN)[21, 22, 24, 25, 26]. However, no studies have investigated whether and how the functional connectome hierarchy is disrupted in patients with MDD. The characterization of the hierarchical architecture of the functional connectome in MDD is highly relevant to an understanding of the network mechanisms underlying the interplay between abnormal sensory and cognitive processing in MDD patients.

Notably, much research has indicated that MDD is a moderately heritable disorder[27]. Genome-wide association studies (GWAS) have identified several risk variants of genes linked to MDD, and some of the replicably identified genes play roles in the biological functions of presynaptic differentiation and neuroinflammation[28]. To date, measuring gene expression in brain tissue *in vivo* has been extremely difficult. The integration of gene expression profiles in the postmortem brain with connectomes derived from neuroimaging data provides unprecedented opportunities to bridge the gap between the microlevel transcriptome profile and the macroscale brain network[18, 29, 30, 31]. The fundamental architectures of functional connectomes (e.g., network hubs) are associated with gene expression profiles involving ion channel activity and oxidative metabolism[30, 32]. Distinct gene expression profiles can also explain the variances in the spatial patterns of alterations in brain structures in different psychiatric states, including schizotypy[33] and autism[34]. If patients with MDD exhibit disturbances in the macroscale connectome hierarchy, we speculate that a microlevel molecular mechanism for coding these functional brain abnormalities might exist.

To address these issues, in the present study we collected a large multisite R-fMRI dataset from 2,234 individuals in China and the postmortem gene expression data from the brains of six donors from the Allen Institute for Brain Science (AIBS)[29]. We investigated the functional connectome hierarchy in MDD and established their associations with the transcriptome profile. Specifically, we hypothesized that (*i*) the connectome hierarchy is disrupted in patients with MDD, where abnormalities exist in both the global hierarchy shapes and regional gradient scores of low-level sensory and high-order transmodal

systems; (*ii*) the regions with an altered connectome hierarchy in MDD are associated with multiple functional domains, including primary processing, such as somatosensory and visual perception, and high-order cognitive functions, such as theory of mind, reward, and working memory; and (*iii*) the spatial patterns of MDD-related hierarchy alterations are associated with gene expression profiles that are enriched in particular biological processes, such as synaptic functions.

Results

This study included R-fMRI data from 2,234 participants (1,150 patients with MDD, 33.8 ± 14.99 years old, 58.5% female; 1,084 HCs, 34.0 ± 13.87 years old, 56.8% female; 622 drag-naïve patients, 54.1%) who were recruited from ten research centers in China through the Disease Imaging Data Archiving - Major Depressive Disorder Working Group (DIDA-MDD; Table 1 and Supplementary Table 1). For each individual, we first constructed high-resolution voxelwise functional connectomes (18,933 nodes) and then applied the diffusion map embedding approach[14, 20] to estimate the connectome hierarchy architecture. The resultant gradient maps were further aligned across individuals using the Procrustes rotation[20] and corrected for the center effect using the ComBat model[6, 35]. We found that the first three gradients explained 28.5% ± 3.9% of the total variance in the connectome across all individuals (MDD, 28.2% ± 3.9%; HC, 28.9% ± 3.9%, Supplementary Fig. 1). The principal gradient (G1) was organized along a gradual axis from the primary visual/sensorimotor networks (VIS/SMN) to the DMN (Fig. 1A), replicating recent findings revealing connectome gradients from the primary to the transmodal cortices in healthy adults[14]. The second gradient (G2) extended between the DMN and the ventral attention network (VAN) and the third gradient (G3) separated the SMN from the VIS network (Fig. 1B and C). The spatial patterns of the group-averaged gradient maps were remarkably similar between the MDD and HC groups, with Spearman's ρ = 0.999, 0.998, and 0.998 for G1, G2, and G3, respectively (all $P <$ 0.00001, Supplementary Fig. 2). Visual inspection of the histogram revealed that the extremes of all three gradients were contracted in MDD relative to the control range (Fig. 1A-C).

Alterations of Connectome Hierarchy in MDD

Statistical between-group comparisons showed that G1 and G3 explained less variance in the functional connectome in the MDD group than in the HC group (P = 0.0002 for G1 and P = 0.019 for G3, Fig. 2A), suggesting a downgraded status of the hierarchal organization in MDD. Moreover, the patients with MDD showed a narrower range of the gradient scores of all three gradients and less spatial variations in G1 and G3 (all $P < 0.0003$, Fig. 2A) than the HCs, indicating a contracted connectome hierarchy in MDD.

To further identify regions with hierarchy alterations, we compared the gradient scores at the voxel-level between MDD and HCs using a general linear model controlling for effects of age and sex. Compared with the HC group, the MDD group showed significantly altered gradient scores (voxel-level $P < 0.001$, Gaussian random field (GRF) cluster level-corrected $P < 0.05$) (Fig. 2B and Supplementary Table 2-4): (*i*) in G1, lower gradient scores in the DMN but higher scores in the VIS and SMN; (*ii*) in G2, lower scores in the DMN but higher scores in the VAN and subcortical regions (SUB); and (*iii*) in G3, lower scores in the FPN but higher scores in the SMN. To synoptically visualize the trajectory of the MDD-related alterations in these regions, we mapped the gradient scores into a space spanned by the three gradients, where the group-averaged gradient scores were anchored in the DMN, VIS, SMN and VAN (Supplementary Fig. 3). The identified clusters, particularly the regions in the DMN, VIS and SMN, showed a strong shift from the periphery to the center in this space, indicating the less-specialized

connectivity profiles of these regions in MDD (Fig. 2C). Moreover, the displacement of these clusters was significantly system dependent ($F = 387.3$, $P < 0.001$), where the VIS, SMN and DMN showed a larger displacement than that expected by chance (all $P < 0.05$, permutation test, Bonferroni corrected, Supplementary Fig. 4).

To further determine the cognitive processes that were most associated with MDD-related gradient alterations, we used Neurosynth (https://neurosynth.org/), a metanalytic tool[36], to decode the thresholded *Z*-maps against cognitive terms derived from experimental task conditions. In Fig. 2D, we found the following: (*i*) the regions with G1 alterations were mainly involved in sensorial and perceptional processes, such as visual, somatosensory and acoustic process, and were activated by DMN-related terms in theory of mind, memory-retrieval, and autobiographical memory; (*ii*) the regions with G2 alterations were best converged with meta-analytic maps of reward, incentive, and reactivity and DMN-related terms; and (*iii*) G3 alterations were located in regions that were activated by perceptional terms and goal-directed task-related performance, including working memory, attention, and maintenance. These results suggest that these gradient alterations are potentially related to abnormal sensory and cognitive processing in patients with MDD.

Associations Between MDD-related Gradient Alterations and Gene Expression Profiles

To explore the potential molecular substrates associated with the MDD-related alterations in the connectome gradients, we used the gene expression datasets of six adult human brain specimens from the AIBS[29]. Partial least squares (PLS) regression was applied to investigate the relationship between the between-group *Z*-maps of the connectome gradients and gene expression profiles. The first component of the PLS regression defined a weighted sum of gene expression that explained 12.5% of the variance in the MDD-related alterations in the connectome gradients ($P < 0.001$, permutation test, Fig. 3A), representing a transcriptional profile characterized by high expression mainly in the posterior parietal-occipital areas but low expression in prefrontal areas (Fig. 3B). The regional mapping of this component positively correlated with the *Z*-map of G1 ($r = 0.551$, $P < 0.001$) but negatively correlated with the *Z*-map of G2 ($r = -0.264$, $P < 0.001$, Fig. 3C). We ranked the genes according to their weights in the PLS model, where the top genes obtained after sorting in descending order were denoted the upregulated set, and those obtained after sorting in ascending order were denoted the downregulated set. Using the Gene Ontology enrichment analysis and visualization tool (GOrilla, http://cbl-gorilla.cs.technion.ac.il/), we found that the downregulated genes were significantly enriched in biological processes related to transsynaptic signaling and molecular function of calcium ion binding (FDR-corrected $q < 0.01$, Fig. 3D and Supplementary Table 5).

Clinical Relations to Connectome Gradients in MDD

Next, we investigated whether the connectome hierarchy was related to clinical variables, including episode number, medication, and onset age in MDD. We divided patients into subgroups according to their clinical variables (i.e., episode, medication, and onset age) and compared the connectome hierarchy metrics between subgroups. Patients in their first episode (N = 512) had a smaller G2 range than recurrent patients (N = 80) ($P = 0.027$, Fig. 4A). Patients with an onset in adolescence (age $\leq$ 21 years, N = 303)[8] showed a significantly narrower gradient range for G1 ($P = 0.001$) and G2 ($P = 0.011$) and a smaller region variation for G1 ($P = 0.026$) than patients who had an onset age older than 21 years (N = 293) (Fig. 4B). There were no significant differences between patients who were and were not taking medication (Supplementary Table 6). Voxelwise comparisons showed that there was no difference in

regional gradient scores between any of these clinical category pairs after correcting for multiple comparisons. We further utilized supervised machine learning[37] to examine whether the connectome gradient features were able to predict depressive symptoms in the patients. Using support vector regression (SVR) and 10-fold cross-validation (where the predictive model was repeatedly trained on 9 folds of the data and tested on the 10th fold), we found that the regional displacement in the gradient space of the clusters with MDD-related alterations could significantly predict the total score of the Hamilton Depression Rating Scale (HDRS; mean average error (MAE) = 5.6, mean $r = 0.15$, $P < 0.0001$, permutation test, Fig. 4C). The most contributive features were located in several primary and high-order systems, such as the SMN (percentage of total feature weights in SVR: 27.2%), DMN (21.1%), and VIS (15.1%) (Fig. 4D and E).

Reproducibility Validation

We estimated the reproducibility of the identified MDD-related gradient alterations by considering several potential confounding factors. First, we used a leave-one-site-out cross- validation strategy to examine whether alterations were associated with specific sites. This was done by repeating the between-group comparisons on the data, excluding one site at a time. Second, some of the participants were younger than 18 years old, which may explain the between-group difference in brain development. Thus, we reperformed the data analysis for only adult participants (1,002 patients with MDD and 1,034 HCs). Finally, to further control for the effect of head motion on R-fMRI connectivity measures, we repeated the between-group comparisons with the mean framewise displacement as an additional covariate. Together, the MDD-related disruption patterns of the connectome gradient remained highly similar to those in our main findings, suggesting a high reproducibility of the results (Supplementary Fig. 5-6 and Supplementary Table 7-8).

Discussion

In this study, based on a large cohort of R-fMRI data, we demonstrated a hierarchical dysfunction in the large-scale functional connectomes in patients with MDD. Specifically, patients with MDD exhibited a downgraded and contracted connectome hierarchy, and the most significant alterations were noted in gradient scores in the sensory and transmodal areas. These gradient changes are tightly associated with transcriptional profiles, and the most correlated genes are enriched in transsynaptic signaling and calcium ion binding. These findings offer insights into the understanding of the neurobiological mechanisms underlying the coexisting deficits in low-level sensory processing and high-order cognitive functions in patients with MDD.

Downgraded and Contracted Connectome Hierarchy in MDD

We identified a downgraded and contracted connectome hierarchy in MDD, indicated by a less-explained variance in the functional connectome and a narrower distribution range of gradient scores. Disturbances in the architecture of the macroscale functional brain network have recently been considered critical in the pathology of depression[21, 38, 39]. Notably, although the changes in the topology of the functional connectomes in MDD remain inconsistent in direction across the literature, likely as a result of differences in patient inclusion criteria and methodological choices[40], many studies have demonstrated a replicable pattern towards a randomized configuration of the functional brain networks in patients with MDD[23, 40, 41]. The downgraded connectome hierarchy in MDD observed here is supported by these prior reports. Randomized network connections can break the natural balance

between integration and segregation in healthy individuals with miswired connections. Therefore, the probability of incomplete or redundant pathway formation for information processing is increased, which results in a less prioritized hierarchical architecture in the functional connectome in MDD. Intriguingly, such an alteration was not the result of the disconnection of a single system but that of widely distributed systems from the low-level primary to the high-order transmodal cortices.

We observed that several specific regions in the SMN/VIS and DMN shifted from the periphery to the center in the hierarchical space, implying a trend towards dedifferentiated connection profiles between these systems. This phenomenon is comparable to previous findings from connectome modular studies in MDD, where hyperconnections were found among the primary visual and sensorimotor systems and the transmodal DMN and FPN[22, 25] and could be used to distinguish remitters from nonremitters[42]. In a hierarchical brain organization, the low-level primary systems receive external stimulation signals and process them into abstract representations[43], while the high-order systems integrate the processed information with internal control, memory, and emotion to guide interactions with the external environment[12, 43]. Specifically, the primary sensory cortices, including the occipital cortex, superior temporal cortex, and postcentral gyrus, have been recognized to play roles in the visual, auditory, and somatosensory systems, particularly for visuospatial, face, language, and perception processes[44, 45, 46]. The core regions of the DMN, such as the medial prefrontal cortex, posterior cingulate cortex, and precuneus, are considered densely connected hubs in the functional connectome and play the most important roles in the theory of mind, memory retrieval, autobiographical memory, and working memory[47, 48, 49]. Consistent with simultaneous clinical and cognitive impairments in multiple domains in MDD, the contracted hierarchy involving multilevel systems in the functional connectome may reflect incomplete or blunt bottom-up information processing from the primary systems and failures in the corresponding top-down processing from the high-order systems[50]. Additionally, the degree of downgrade and contraction in the connectome hierarchy increases as the patient onset age decreases, indicating that an early onset is linked with more severe changes in the connectome hierarchy. A recent study showed that the principal DMN-SMN/VIS gradient pattern observed in healthy adults is not fully developed in neonates[19]. Therefore, the early onset of MDD in childhood and adolescence may have an interactive effect on the development of the connectome hierarchy, which needs to be studied in the future.

Gene Expression Profiles for Transsynaptic Signaling and Calcium Ion Binding in MDD

Our connectome-transcriptome association analysis established a link between MDD-related changes in connectome gradients and gene expression enriched in transsynaptic signaling and calcium ion binding. Transsynaptic signaling is one of the most fundamental biological processes that contributes to a series of critical molecular functions, including instructing the formation of synapses, regulating synaptic plasticity, and matching pre- and postsynaptic neurons[51, 52]. It enables the establishment of complex neuronal networks supporting effective information transfer and processing throughout the brain. The variation in synaptic signaling across the cerebral cortex has been demonstrated to be organized along the axis of the cortical hierarchy, which corresponds well to the principal gradient of macroscale functional connectomes[17, 53]. Notably, disruptions in transsynaptic signaling in many of the key pathways can influence the formation and stability of synapses and have been known to play roles in the pathology of depression[54]. For example, studies in postmortem tissues and rodent models revealed that exposure to chronic stress can disrupt the pathway of brain-derived neurotrophic factor (BDNF)-tropomyosin-related kinase B (TrkB) receptor signaling by reducing the downstream extracellular signal-regulated kinase (ERK) and Akt pathways in the hippocampus and prefrontal cortex[55, 56].

Disturbances in these pathways can decrease the expression and function of BDNF and further cause neuronal atrophy in regions that are implicated in depression[57]. Consistent with our findings, a recent study combining gene coexpression networks and genome-wide summary statistics also revealed that MDD risk genes were enriched in gene modules involving transsynaptic signaling[58]. In addition to transsynaptic signaling, calcium ion binding is another crucial molecular function for intracellular signaling. In particular, calcium ion binding can occur in signal transduction resulting from the activation of ion channels or as a second messenger in wide-ranging physiological pathways involving synaptic plasticity. In MDD, evidence from postmortem studies suggests that the density of calbindin-immunoreactive GABAergic neurons is significantly reduced in the dorsolateral prefrontal cortex of the patients[59]. Here, our findings provide further evidence that the disrupted connectome hierarchy architecture in MDD is associated with the gene expression profile related to these two general molecular mechanisms. However, we were unable to determine whether microlevel transcriptional dysregulation resulted in macrolevel connectome dysfunction or whether either of these were causally influenced by risk factors for MDD, such as environmental risk factors.

Limitations and Further Considerations

First, cognitive performance was not fully recorded for each patient, which limited the opportunity to study the associations between connectome hierarchy disruptions and different aspects of cognitive domains in MDD. Alternatively, we compared the gradient alteration maps to the meta-analytic cognitive topic maps from the widely used Neurosynth database[36] to illustrate cognitive terms. Second, longitudinal treatment datasets of MDD were not included in the current study. Previous studies have suggested that the functional brain abnormalities can be normalized after anti-depressant[60], electroconvulsive therapy[61], or deep brain stimulation surgery[62] in patients with MDD. Future studies using longitudinal datasets are critical for understanding the effects of treatment on connectome hierarchy architectures in MDD and for providing imaging biomarkers for evaluating treatment effects. Finally, the gene expression data from the AIBS were sampled from donors without a diagnosis of MDD. Thus, the observed association between connectome hierarchy and transcriptome profiles should be considered cautiously. Future studies with larger samples of whole-brain genome-wide gene expression data for MDD could provide stronger evidence to address this issue.

Materials and Methods

Imaging Dataset

This study included 2,414 participants (1,276 patients with MDD and 1,138 HCs) who were recruited from ten research centers in China through the DIDA-MDD (China Medical University, CMU; Central South University, CSU; Guangzhou University of Chinese Medicine, GCMU (two datasets); Kunming Medical University, KMU; Peking University Sixth Hospital, PKU; Sichuan University, SCU; Southwest University, SWU; National Yang-Ming University, YMU; and Zhengzhou University, ZZU). All patients were diagnosed according to the Diagnostic and Statistical Manual of Mental Disorders IV (DSM-IV) criteria for MDD[63] but not for any other Axis I disorders. The severity of depression was rated using the HDRS[64]. The HCs did not have a current or lifetime history of any Axis I disorder. The exclusion criteria for all participants included MRI contraindications, a history of drug or alcohol abuse, concomitant major medical disorders, head trauma with consciousness disturbances or any neurological disorders. Quality control was performed for both clinical and imaging data, and 180 participants were excluded due to a lack of demographic information (N = 5), age (7 years old, N = 1), a change in their diagnosis during follow-up interviews (N = 7), duplicate data in the data transfer or errors in the raw DICOM data (N = 10), different scanning parameters or incomplete scans (N = 24), abnormalities in the anatomical brain images (N = 14), excessive head motion (exceeding 3 mm of translational movement, 3° of rotational movement or 0.5 mm of mean framewise displacement, N = 71), incomplete coverage of the entire brain (N = 46), error in normalization (N = 1), and an abnormal temporal signal-to-noise ratio (N = 1). The final sample included 2,234 participants (1,150 patients with MDD and 1,084 HCs, Table 1). The study was approved by the ethics committees of each center, and written informed consent was obtained from each participant. The R-fMRI data of all participants were obtained on 3.0-T MRI scanners with gradient-echo planar imaging sequences. During the scan, the participants were instructed to keep their eyes closed without falling asleep and to move as little as possible. Detailed scanning parameters for each center are listed in Supplementary Table 1. A subset of the dataset was used to study regional activity and functional connectivity in MDD[6] but not connectome gradients.

Data Preprocessing

R-fMRI image preprocessing was conducted with SPM12 (www.fil.ion.ucl.ac.uk/spm/) and SeeCAT (www.nitrc.org/projects/seecat), an in-house toolbox. Briefly, the first ten time points (the first five time points for the CSU, GCMU1 and ZZU datasets due to their short scan times) were discarded. Subsequent preprocessing steps included slice-timing correction and head-motion correction. Next, the motion-corrected functional images were normalized to the standard space using an echo planar imaging (EPI) template, resampled to 3-mm isotropic voxels, and further smoothed with a 6-mm full-width at half-maximum Gaussian kernel. Linear detrending was performed, and several confounding covariates, including the Friston-24 head-motion parameters and the white matter and cerebrospinal fluid signals, were regressed out from the time series for all voxels. Subsequently, temporal bandpass filtering (0.01-0.08 Hz) was applied. Finally, a "scrubbing" procedure was performed on individual preprocessed datasets to remove outlier data due to head motion[65]. Specifically, for volumes with a framewise displacement exceeding a threshold of 0.5 mm, we replaced the volumes and their adjacent volumes (2 forward and 1 backward frames) with linearly interpolated data.

Connectome Hierarchy Analysis

We constructed individual functional connectomes at the voxel level. To reduce the computational complexity, we resampled the preprocessed R-fMRI images to a 4-mm isotropic resolution. For each individual, a functional connectivity matrix was first estimated by calculating the Pearson correlation coefficients between each pair of gray matter nodes (18,933 voxels). The top 10% of the connections were retained for each node, and the cosine similarity was calculated between each pair of nodes. The similarity matrix was further scaled into a normalized angle matrix to avoid negative values[19, 66]. Then, diffusion map embedding was applied to capture the gradient components that could explain the variance in the connectivity pattern of the functional connectome. Following the previous recommendation, we set the manifold learning parameter $\alpha = 0.5$[14, 19, 20]. For each gradient map, the explanation ratio for the connectome variance, distribution range and spatial variance were calculated. Procrustes rotation was performed to align individual gradient maps across subjects[19, 20]. Finally, we utilized the ComBat model, an empirical Bayes-based multivariate linear mixed-effects regression, to correct for site effects on the gradient map and measurements[6, 35]. The between-group differences in the gradient measurements were determined by two-sample *t* test with age and sex controlled. The significance level of the voxelwise comparison was set to a voxel-level $P < 0.001$ with a cluster-level Gaussian random field-corrected $P < 0.05$.

Cognitive Topics Relevant to Alterations in Gradients in MDD

We used Neurosynth (https://neurosynth.org/)[36] to assess the topic terms associated with the alterations in the connectome gradient in MDD. The thresholded *Z*-maps derived from the between-group comparisons for each gradient were first divided into MDD-positive and MDD-negative maps. The resultant maps were then uploaded to Neurovault and analyzed using the "decoder" function of Neurosynth website. For each of the maps, the noncognitive terms (e.g., anatomical and demographic terms) were removed and the top 30 cognitive terms were selected. The cognitive terms were visualized on a word-cloud plot with the font size scaled according to their correlation with corresponding meta-analytic maps generated by Neurosynth.

Gene Expression Dataset

The microarray-based gene expression data of the Human Brain Atlas were downloaded from the AIBS website[29]. The human brain tissue samples in this atlas were collected from the brains of six adult donors (mean age: 42.5 years, 1 female), including two complete brains and four left hemispheres. Each postmortem hemisphere of the brain had been dissected into approximately 500 anatomically discrete samples. Each sample had been spatially registered to the Montreal Neurological Institute (MNI) coordinate space according to the T1-weighted images obtained before dissection, and the locations of all samples are given in MNI coordinates. Normalization processes were conducted by the AIBS to minimize the potential effects of nonbiological biases and ensure the gene expression data were comparable among samples within and across the brains.

Gene Expression Data Preprocessing

Given that the AIBS dataset did not cover the whole brain at the voxel level, we utilized cortical 360-region brain parcellation[18, 67] to perform gradient-gene expression association analysis. We performed preprocessing for the gene expression microarray data of brain tissue samples by using the Allen Human

Brain Atlas (AHBA) processing pipeline (https://github.com/BMHLab/AHBAprocessing) with the default recommended setting[68]. This preprocessing procedure is built on a systematic assessment of workflow for combining AHBA and neuroimaging data[68]. Briefly, the probe-to-gene annotations were verified using the hg38 sequencing database. Then, probes with values that did not exceed background noise were filtered. The probe with the highest correlation to RNA-seq data was selected to index expression for a gene. Then, each tissue sample was assigned to its nearest cortical region of the 360-parcellation. Samples with a distance greater than 2 mm to any of the 360 regions were excluded. These procedures resulted in 820 brain tissue samples covering 284 regions with each sample containing the expressions of 10,027 genes. Subsequently, a two-step scaled robust sigmoid normalization approach was used to correct for both intersample and intersubject variability. For each sample, normalization was applied across all the probes within the sample. Then, for each subject, normalizations were performed for each probe across all the samples. Finally, for each region, the gene expression was obtained by averaging all samples from six donors, resulting in a gene expression map (284 regions × 10,027). Four regions were excluded in the following analysis due to the low overlapping percentage (< 50%) between the cortical 360-region brain parcellation and the gray matter mask in this study.

Association Analysis Between Gradient Alterations and Gene Expression

We used partial least squares (PLS) regression to explore the association between transcriptional profiles and the alterations in the connectome gradients in MDD. PLS regression can define several components, each of which is a linear combination of the predictor variables (i.e., gene expression) that can explain most of the variance in the response variables (i.e., between-group difference *t*-maps of connectome gradients). The predictor variables matrix X and the response variables matrix Y are first centered, resulting in X_0 and Y_0, respectively. Component i of the PLS regression is then weighted by p_i and q_i to calculate the component scores T_i and U_i for X_0 and Y_0, respectively:

$$T_i = X_0 p_i + E; U_i = Y_0 q_i + F$$

where E and F are error terms. Then, the weight vectors p_i and q_i and the component scores T_i and U_i are estimated to ensure the maximum covariance between T_i and U_i. Thus, the regression of the predictor variables and response variables can be defined as follows:

$$U_i \sim T_i \text{ or } Y_0 q_i = B_{0i} + B_{1i} X_0 p_i + G$$

where G is an error term and B_{1i} and B_{0i} are the regression coefficient and intercept, respectively. The R^2 of the fitting for each component illustrates how much the predictive variables can explain the variance in the response variables. Here, in our PLS model, the gene expression data of the brain nodes (280 nodes × 10,027 genes) were set as the predictor variables X, and the Z values of gradient gradients 1, 2, and 3 of the brain nodes (280 nodes × 3 statistics) were set as the response variables Y.

A permutation test was performed to determine whether the R^2 derived from PLS regression analysis was significantly greater than that expected by chance. In each permutation, the labels of the nodes of the response variables were shuffled, and surrogate Z values were assigned to each node. Then, the surrogate Z values were used as the response variable in the PLS regression, and the corresponding R^2

values were recorded. The permutation was repeated 10,000 times to generate the null model. The real R^2 values of the first few components that explained over ten percent of the variance in the response variables (here, only one component over ten percent) were compared with those from this null model to determine whether the real R^2 values were significantly greater than those expected by chance. Then, for each significant component, we used a bootstrapping method to assess the estimation error of the weight of each gene and further divided the weight by the estimated error to obtain the corrected weight of each gene[69].

We ranked the genes according to their corrected weights, which represent their contribution to the PLS regression components. Both the positive and negative sequences were enrolled for the following gene enrichment analysis. The Gene Ontology enrichment analysis and visualization tool (GOrilla, http://cbl-gorilla.cs.technion.ac.il/)[70] was used to identify the enriched Gene Ontology terms of the ranked genes from each significant component. Specifically, we used a *P*-value threshold of 10^{-6} in the advanced parameter settings and applied the Benjamini-Hochberg false discovery rate (FDR) method to correct for the multiple tests. In the main results, the Gene Ontology terms with an FDR *q*-value less than 0.01 were reported. The Reduce Visualize Gene Ontology (REVIGO, http://revigo.irb.hr/) tool was used to summarize the obtained Gene Ontology terms by removing redundant terms.

Predicting Individual Depressive Symptoms with a Machine Learning Model

We performed support vector regression (SVR) with a linear kernel to examine the ability of the connectome gradients to predict patient symptoms. A 10-fold cross-validation strategy was adopted to estimate the accuracy of the prediction. Here, the participants were first sorted according to their HDRS scores and were then assigned to the corresponding fold (e.g., 1st, 11th, …, to the first fold; 2nd, 12th, …, to the second fold; 3rd, 13th, …, to the third fold; etc.). Nine folds of the data were defined as the training set in turn, and the remaining fold was defined as the test set. During each training procedure, an internal 5-fold cross-validation was performed to optimize the parameters of the SVR with a grid search (i.e., C = 10^{-3}, 10^{-2}, 10^{-1}, 10^{0}, 10^{1}, 10^{2}, 10^{3}, 10^{4}, and 10^{5}). To avoid the bias caused by features with greater numeric ranges, we linearly scaled each feature to the range of 0–1 across the training dataset, and applied the estimated scaling parameters to the testing dataset. The final accuracy was reported as the Pearson's correlation coefficient between the predicted and observed HDRS scores across all patients. The nonparametric permutation test (10,000 times) was performed to assess the statistical significance of the prediction accuracy. During each permutation, the observed HDRS scores of the patients were randomly shuffled prior to SVR and cross-validation. Thus, the null distribution of the correlation coefficients was obtained, and a *P*-value was calculated by dividing the number of times that the permutations had higher correlation coefficients than the real coefficient by 10,000. The codes for this prediction analysis were mainly modified from Cui and Gong [71] (https://github.com/ZaixuCui/Pattern_Regression_Matlab) and the libsvm (www.csie.ntu.edu.tw/~cjlin/libsvm/).

Data availability

The data collected and analyzed during the current study are available from the corresponding author on reasonable request. All relevant codes are publicly available upon publication.

References:

1. DALYs GBD, Collaborators H. Global, regional, and national disability-adjusted life-years (DALYs) for 359 diseases and injuries and healthy life expectancy (HALE) for 195 countries and territories, 1990-2017: a systematic analysis for the Global Burden of Disease Study 2017. *Lancet* **392**, 1859-1922 (2018).
2. Northoff G, Hirjak D, Wolf RC, Magioncalda P, Martino M. All roads lead to the motor cortex: psychomotor mechanisms and their biochemical modulation in psychiatric disorders. *Molecular psychiatry*, (2020).
3. Miller CH, Hamilton JP, Sacchet MD, Gotlib IH. Meta-analysis of Functional Neuroimaging of Major Depressive Disorder in Youth. *JAMA Psychiatry* **72**, 1045-1053 (2015).
4. Hamilton JP, Farmer M, Fogelman P, Gotlib IH. Depressive Rumination, the Default-Mode Network, and the Dark Matter of Clinical Neuroscience. *Biol Psychiatry* **78**, 224-230 (2015).
5. Millan MJ*, et al.* Cognitive dysfunction in psychiatric disorders: characteristics, causes and the quest for improved therapy. *Nat Rev Drug Discov* **11**, 141-168 (2012).
6. Xia M*, et al.* Reproducibility of functional brain alterations in major depressive disorder: Evidence from a multisite resting-state functional MRI study with 1,434 individuals. *Neuroimage* **189**, 700-714 (2019).
7. Cheng W*, et al.* Medial reward and lateral non-reward orbitofrontal cortex circuits change in opposite directions in depression. *Brain* **139**, 3296-3309 (2016).
8. Schmaal L*, et al.* Cortical abnormalities in adults and adolescents with major depression based on brain scans from 20 cohorts worldwide in the ENIGMA Major Depressive Disorder Working Group. *Molecular psychiatry* **22**, 900-909 (2017).
9. van Velzen LS*, et al.* White matter disturbances in major depressive disorder: a coordinated analysis across 20 international cohorts in the ENIGMA MDD working group. *Molecular psychiatry* **25**, 1511-1525 (2020).
10. Singh MK*, et al.* Anomalous gray matter structural networks in major depressive disorder. *Biol Psychiatry* **74**, 777-785 (2013).
11. Meng C*, et al.* Aberrant topology of striatum's connectivity is associated with the number of episodes in depression. *Brain* **137**, 598-609 (2014).
12. Mesulam MM. From sensation to cognition. *Brain* **121 (Pt 6)**, 1013-1052 (1998).
13. Biswal B, Yetkin FZ, Haughton VM, Hyde JS. Functional connectivity in the motor cortex of resting human brain using echo-planar MRI. *Magn Reson Med* **34**, 537-541 (1995).
14. Margulies DS*, et al.* Situating the default-mode network along a principal gradient of macroscale cortical organization. *Proc Natl Acad Sci U S A* **113**, 12574-12579 (2016).
15. Huntenburg JM, Bazin PL, Margulies DS. Large-Scale Gradients in Human Cortical Organization. *Trends Cogn Sci* **22**, 21-31 (2018).
16. Huntenburg JM, Bazin PL, Goulas A, Tardif CL, Villringer A, Margulies DS. A Systematic Relationship Between Functional Connectivity and Intracortical Myelin in the Human Cerebral Cortex. *Cereb Cortex* **27**, 981-997 (2017).
17. Burt JB*, et al.* Hierarchy of transcriptomic specialization across human cortex captured by structural neuroimaging topography. *Nat Neurosci* **21**, 1251-1259 (2018).

18. Liu J, Xia M, Wang X, Liao X, He Y. The spatial organization of the chronnectome associates with cortical hierarchy and transcriptional profiles in the human brain. *Neuroimage* **222**, 117296 (2020).

19. Lariviere S*, et al.* Multiscale Structure-Function Gradients in the Neonatal Connectome. *Cereb Cortex* **30**, 47-58 (2020).

20. Hong SJ*, et al.* Atypical functional connectome hierarchy in autism. *Nature communications* **10**, 1022 (2019).

21. Gong Q, He Y. Depression, neuroimaging and connectomics: a selective overview. *Biol Psychiatry* **77**, 223-235 (2015).

22. Ma Q*, et al.* Transdiagnostic Dysfunctions in Brain Modules Across Patients with Schizophrenia, Bipolar Disorder, and Major Depressive Disorder: A Connectome-Based Study. *Schizophr Bull* **46**, 699-712 (2020).

23. Xia M*, et al.* Shared and Distinct Functional Architectures of Brain Networks Across Psychiatric Disorders. *Schizophr Bull* **45**, 450-463 (2019).

24. Yan CG*, et al.* Reduced default mode network functional connectivity in patients with recurrent major depressive disorder. *Proc Natl Acad Sci U S A* **116**, 9078-9083 (2019).

25. Yu M*, et al.* Childhood trauma history is linked to abnormal brain connectivity in major depression. *Proc Natl Acad Sci U S A* **116**, 8582-8590 (2019).

26. Kaiser RH, Andrews-Hanna JR, Wager TD, Pizzagalli DA. Large-Scale Network Dysfunction in Major Depressive Disorder: A Meta-analysis of Resting-State Functional Connectivity. *JAMA Psychiatry* **72**, 603-611 (2015).

27. Flint J, Kendler KS. The Genetics of Major Depression. *Neuron* **81**, 1214 (2014).

28. Wray NR*, et al.* Genome-wide association analyses identify 44 risk variants and refine the genetic architecture of major depression. *Nat Genet* **50**, 668-681 (2018).

29. Hawrylycz MJ*, et al.* An anatomically comprehensive atlas of the adult human brain transcriptome. *Nature* **489**, 391-399 (2012).

30. Richiardi J*, et al.* BRAIN NETWORKS. Correlated gene expression supports synchronous activity in brain networks. *Science* **348**, 1241-1244 (2015).

31. Fornito A, Arnatkeviciute A, Fulcher BD. Bridging the Gap between Connectome and Transcriptome. *Trends Cogn Sci* **23**, 34-50 (2019).

32. Vertes PE*, et al.* Gene transcription profiles associated with inter-modular hubs and connection distance in human functional magnetic resonance imaging networks. *Philos Trans R Soc Lond B Biol Sci* **371**, (2016).

33. Romero-Garcia R*, et al.* Schizotypy-Related Magnetization of Cortex in Healthy Adolescence Is Colocated With Expression of Schizophrenia-Related Genes. *Biol Psychiatry* **88**, 248-259 (2020).

34. Romero-Garcia R, Warrier V, Bullmore ET, Baron-Cohen S, Bethlehem RAI. Synaptic and transcriptionally downregulated genes are associated with cortical thickness differences in autism. *Molecular psychiatry* **24**, 1053-1064 (2019).

35. Yu M*, et al.* Statistical harmonization corrects site effects in functional connectivity measurements from multi-site fMRI data. *Hum Brain Mapp* **39**, 4213-4227 (2018).

36. Yarkoni T, Poldrack RA, Nichols TE, Van Essen DC, Wager TD. Large-scale automated synthesis of human functional neuroimaging data. *Nature methods* **8**, 665-670 (2011).

37. Sui J, Jiang R, Bustillo J, Calhoun V. Neuroimaging-based Individualized Prediction of Cognition and Behavior for Mental Disorders and Health: Methods and Promises. *Biol Psychiatry*, (2020).

38. Malhi GS, Mann JJ. Depression. *Lancet* **392**, 2299-2312 (2018).

39. Qiu L*, et al.* Characterization of major depressive disorder using a multiparametric classification approach based on high resolution structural images. *Journal of psychiatry & neuroscience : JPN* **39**, 78-86 (2014).

40. Borchardt V*, et al.* Preprocessing strategy influences graph-based exploration of altered functional networks in major depression. *Hum Brain Mapp* **37**, 1422-1442 (2016).

41. Zhang J*, et al.* Disrupted brain connectivity networks in drug-naive, first-episode major depressive disorder. *Biol Psychiatry* **70**, 334-342 (2011).

42. Korgaonkar MS, Goldstein-Piekarski AN, Fornito A, Williams LM. Intrinsic connectomes are a predictive biomarker of remission in major depressive disorder. *Molecular psychiatry* **25**, 1537-1549 (2020).

43. Taylor P, Hobbs JN, Burroni J, Siegelmann HT. The global landscape of cognition: hierarchical aggregation as an organizational principle of human cortical networks and functions. *Scientific reports* **5**, 18112 (2015).

44. Srimal R, Curtis CE. Persistent neural activity during the maintenance of spatial position in working memory. *Neuroimage* **39**, 455-468 (2008).

45. Perrodin C, Kayser C, Abel TJ, Logothetis NK, Petkov CI. Who is That? Brain Networks and Mechanisms for Identifying Individuals. *Trends Cogn Sci* **19**, 783-796 (2015).

46. Romo R, Rossi-Pool R. Turning Touch into Perception. *Neuron* **105**, 16-33 (2020).

47. Buckner RL, Andrews-Hanna JR, Schacter DL. The brain's default network: anatomy, function, and relevance to disease. *Ann N Y Acad Sci* **1124**, 1-38 (2008).

48. Liu J*, et al.* Intrinsic Brain Hub Connectivity Underlies Individual Differences in Spatial Working Memory. *Cereb Cortex* **27**, 5496-5508 (2017).

49. Liang X, Zou Q, He Y, Yang Y. Coupling of functional connectivity and regional cerebral blood flow reveals a physiological basis for network hubs of the human brain. *Proc Natl Acad Sci U S A* **110**, 1929-1934 (2013).

50. Kendler KS. The Origin of Our Modern Concept of Depression-The History of Melancholia From 1780-1880: A Review. *JAMA Psychiatry* **77**, 863-868 (2020).

51. Fossati M*, et al.* Trans-Synaptic Signaling through the Glutamate Receptor Delta-1 Mediates Inhibitory Synapse Formation in Cortical Pyramidal Neurons. *Neuron* **104**, 1081-1094 e1087 (2019).

52. de Wit J, Ghosh A. Specification of synaptic connectivity by cell surface interactions. *Nat Rev Neurosci* **17**, 22-35 (2016).

53. Wang XJ. Macroscopic gradients of synaptic excitation and inhibition in the neocortex. *Nat Rev Neurosci* **21**, 169-178 (2020).

54. Duman RS, Aghajanian GK. Synaptic dysfunction in depression: potential therapeutic targets. *Science* **338**, 68-72 (2012).

55. Duman RS, Voleti B. Signaling pathways underlying the pathophysiology and treatment of depression: novel mechanisms for rapid-acting agents. *Trends Neurosci* **35**, 47-56 (2012).

56. Duric V*, et al.* A negative regulator of MAP kinase causes depressive behavior. *Nat Med* **16**, 1328-1332 (2010).

57. Krishnan V, Nestler EJ. The molecular neurobiology of depression. *Nature* **455**, 894-902 (2008).

58. Gerring ZF, Gamazon ER, Derks EM, Major Depressive Disorder Working Group of the Psychiatric Genomics C. A gene co-expression network-based analysis of multiple brain tissues reveals novel genes and molecular pathways underlying major depression. *PLoS Genet* **15**, e1008245 (2019).

59. Rajkowska G, O'Dwyer G, Teleki Z, Stockmeier CA, Miguel-Hidalgo JJ. GABAergic neurons immunoreactive for calcium binding proteins are reduced in the prefrontal cortex in major depression. *Neuropsychopharmacology : official publication of the American College of Neuropsychopharmacology* **32**, 471-482 (2007).

60. Wang L*, et al.* The effects of antidepressant treatment on resting-state functional brain networks in patients with major depressive disorder. *Hum Brain Mapp* **36**, 768-778 (2015).

61. Perrin JS*, et al.* Electroconvulsive therapy reduces frontal cortical connectivity in severe depressive disorder. *Proc Natl Acad Sci U S A* **109**, 5464-5468 (2012).

62. Mayberg HS*, et al.* Deep brain stimulation for treatment-resistant depression. *Neuron* **45**, 651-660 (2005).

63. First M, Spitzer R, Gibbon M, Williams J. *Structured Clinical Interview for DSM-IV Axis I Disorders.* American Psychiatric Publishing (1997).

64. Williams JB. A structured interview guide for the Hamilton Depression Rating Scale. *Arch Gen Psychiatry* **45**, 742-747 (1988).

65. Power JD, Barnes KA, Snyder AZ, Schlaggar BL, Petersen SE. Spurious but systematic correlations in functional connectivity MRI networks arise from subject motion. *Neuroimage* **59**, 2142-2154 (2012).

66. Paquola C*, et al.* Microstructural and functional gradients are increasingly dissociated in transmodal cortices. *PLoS Biol* **17**, e3000284 (2019).

67. Glasser MF*, et al.* A multi-modal parcellation of human cerebral cortex. *Nature* **536**, 171-178 (2016).

68. Arnatkeviciute A, Fulcher BD, Fornito A. A practical guide to linking brain-wide gene expression and neuroimaging data. *Neuroimage* **189**, 353-367 (2019).

69. Whitaker KJ*, et al.* Adolescence is associated with genomically patterned consolidation of the hubs of the human brain connectome. *Proc Natl Acad Sci U S A* **113**, 9105-9110 (2016).

70. Eden E, Navon R, Steinfeld I, Lipson D, Yakhini Z. GOrilla: a tool for discovery and visualization of enriched GO terms in ranked gene lists. *BMC Bioinformatics* **10**, 48 (2009).

71. Cui Z, Gong G. The effect of machine learning regression algorithms and sample size on individualized behavioral prediction with functional connectivity features. *Neuroimage* **178**, 622-637 (2018).

72. Xia M, Wang J, He Y. BrainNet Viewer: a network visualization tool for human brain connectomics. *PLoS One* **8**, e68910 (2013).

73. Yeo BT*, et al.* The organization of the human cerebral cortex estimated by intrinsic functional connectivity. *J Neurophysiol* **106**, 1125-1165 (2011).

Acknowledgements

This work was supported by the National Natural Science Foundation of China (81671767, 82071998, 81620108016, 91432115, 81630031, 31771231, 31271087, 81271499, 81571311, 81571331, 81571331, 81171286, 91232714, 81621003, 81920108019, 81771344, and 81660237), Fundamental Research Funds for the Central Universities (2020NTST29), the National Key R&D Program of China (2018YFA0701400), the Changjiang Scholar Professorship Award (T2015027), the Beijing Nova Program (Z191100001119023), the National High Tech Development Plan (863) (2015AA020513), the National Science and Technologic Program of China (2015BAI13B02), the National Basic Research Program of China (2013CB835100), the Natural Science Foundation of Chongqing (cstc2019jcyj-msxmX0520), the Medical Science and Technology Research Project of Henan Province (201701011), and Shanghai Science and Technology Innovation Plan (17JC1404105 and 17JC1404101). The authors thank the Allen Institute for Brain Science for providing the gene expression data.

Author contributions

M.X. and Y.H. designed research; X.W., D.W., Y.Chen, B.L., C.-C.H., Y.Z., Y.W., T.C., Y.Cheng, X.X., Q.G., T.S., S.Q., C.-P.L., J.C., Y.T., F.W., J.Q., P.X., and L.L. collected data; M.X., X.S., and Q.M. performed data quality control; M.X., and J.L., analyzed data; and M.X., J.L., and Y.H., wrote the paper.

Competing interests

The authors declare no competing interests.

Figure Legends

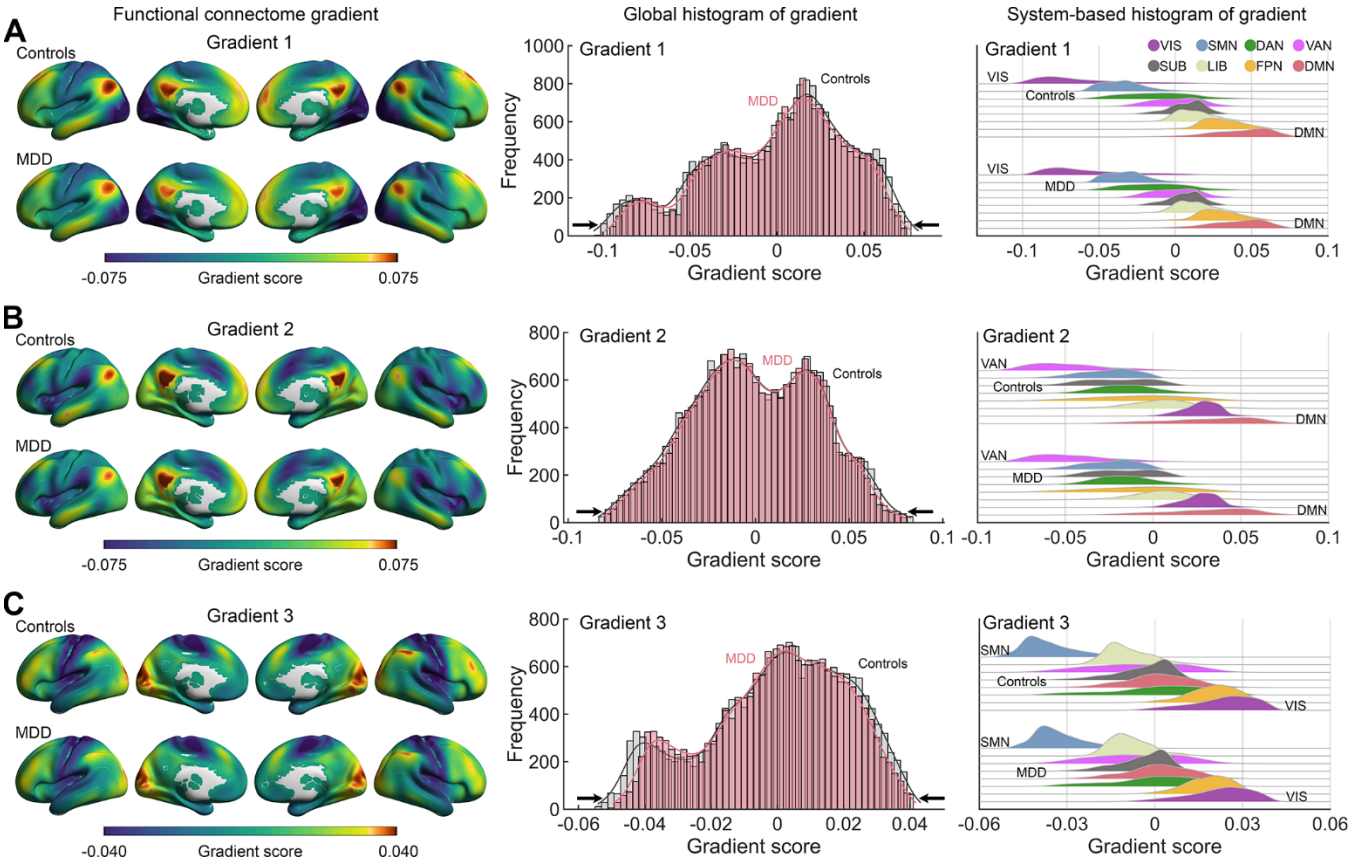

Fig. 1. Connectome gradient mapping in patients with MDD and controls. **(A)** The principal gradient was organized along a gradual axis from the primary visual/sensorimotor networks to the default mode network. **(B)** The second gradient extended between the default mode and the ventral attention networks. **(C)** The third gradient separated the sensorimotor from the visual networks. Global and system-based histograms show that the extreme values were contracted in patients with MDD relative to the controls for all three gradients. Surface rendering was generated using BrainNet Viewer (www.nitrc.org/projects/bnv/)[72] with the inflated cortical 32K surface[67]. VIS, visual network; SMN, sensorimotor network; DAN, dorsal attention network; VAN, ventral attention network; SUB, subcortical regions; LIB, limbic network; FPN, frontoparietal network; DMN, default mode network.

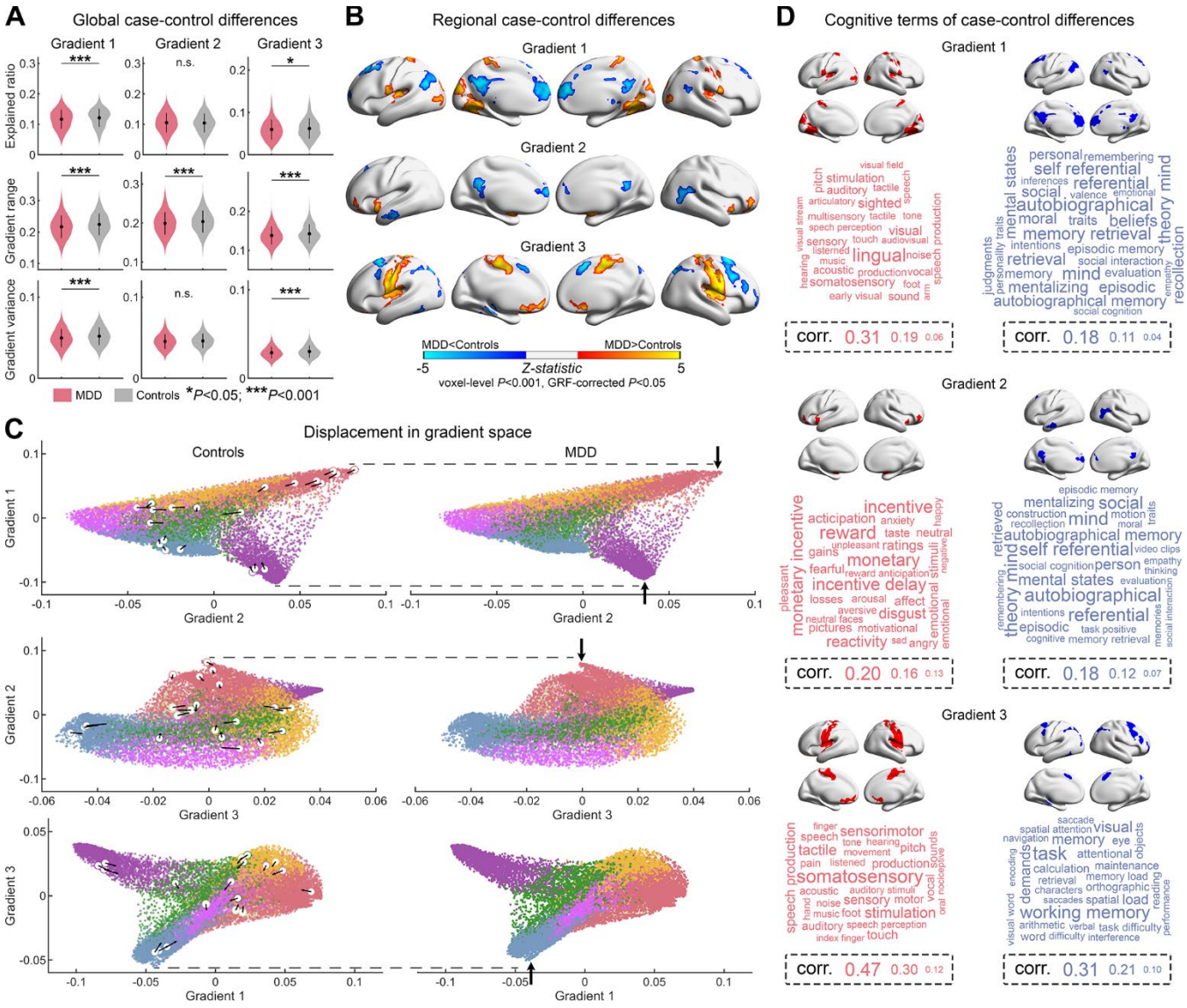

Fig. 2. Statistical comparison of gradient metrics. **(A)** Case-control differences in global gradient metrics. *, $P < 0.05$; ***, $P < 0.001$; n.s., not significant. **(B)** Voxelwise statistical comparisons between controls and patients with MDD, and higher/lower values in MDD are presented as warm/cold colors. The significance level was set as voxel-level $P < 0.001$ and Gaussian random field cluster level-corrected $P < 0.05$. **(C)** Scatter plot for each pair of the first three gradients in controls and patients with MDD illustrates a contracted distribution of gradient scores in MDD. Each dot represents a voxel and its color indicates the corresponding system. The circles represent the peak of the clusters with case-control differences and indicate their displacement from the periphery to the center in this space. **(D)** Word clouds of cognitive terms associated with brain regions that exhibited higher (red) or lower (blue) gradient scores in MDD. The font size of the cognitive terms corresponds to the correlation of corresponding meta-analytic maps generated by Neurosynth.

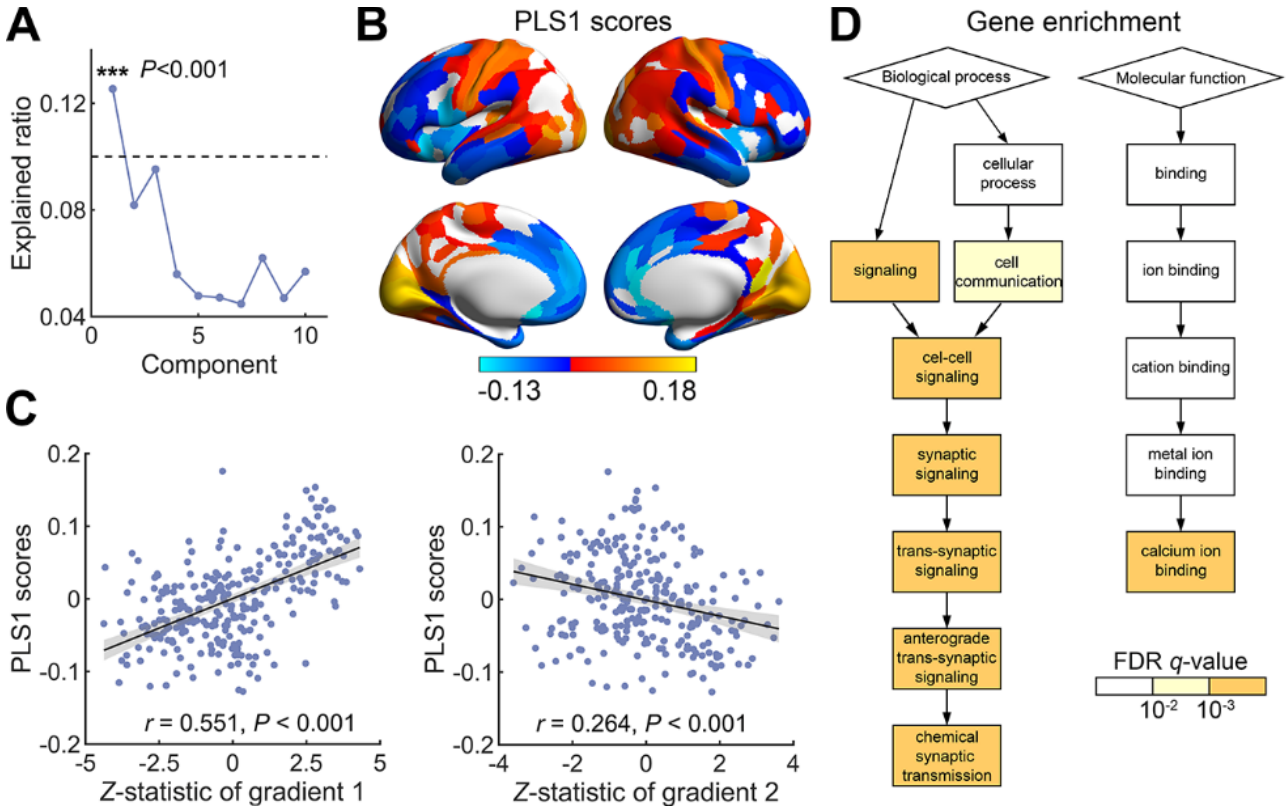

Fig. 3. Association between MDD-related gradient alterations and gene expression. **(A)** The percentage of variance in response variables explained by components in the partial least squares regression analysis. ***, $P < 0.001$. **(B)** The first partial least squares component (PLS 1) identified a gene expression profile with high expression mainly in the posterior parietal-occipital areas but low expression in prefrontal areas. **(C)** This transcriptional profile was positively correlated with the between-group *Z*-map of Gradient 1 but negatively correlated with the between-group *Z*-map of Gradient 2. The shadow indicates 95% confidence intervals. Each dot represents a region. **(D)** The inversed gene rank of PLS 1 is enriched for genes related to Gene Ontology of the biological process of trans-synaptic signaling and molecular function of calcium ion binding.

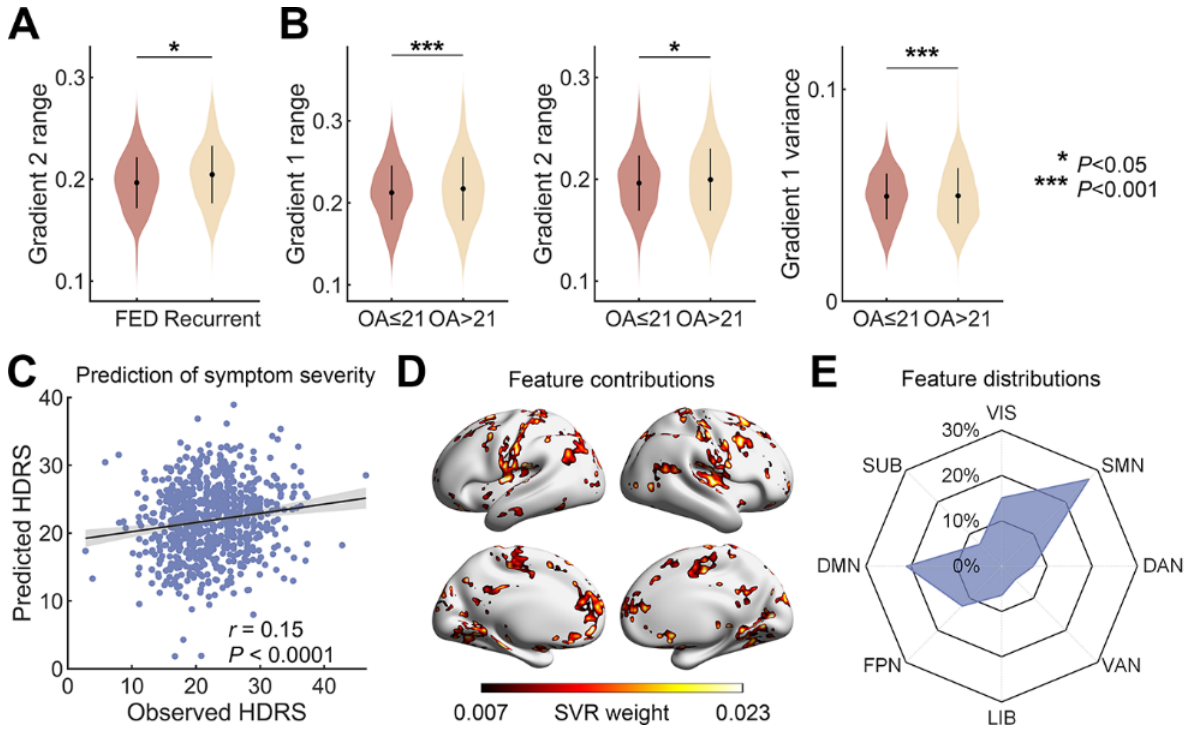

Fig. 4. Clinical influences and symptom prediction. **(A)** Group differences in the range of Gradient 2 between patients in their first-episode and recurrent patients. **(B)** Group differences in the range of Gradient 1 and Gradient 2 and variance of Gradient 1 between patients with an onset age ≤ 21 years and those with an onset age of older than 21 years. *, $P < 0.05$; ***, $P < 0.001$. **(C)** Scatter plot presents significant positive correlations between the observed Hamilton Depression Rating Scale and the predicted scores derived from the SVR analysis with 10-fold cross-validation using MDD-related displacement in gradient space as features (permutation-tests; $P < 0.0001$). Each dot represents the data from one patient, and the dashes indicate the 95% prediction error bounds. **(D)** The absolute weight in 10-fold cross-validation were summed and mapped onto brain surface. Regions with higher/lower predictive power were colored in white/red. **(E)** The radar map represents the distribution of predictive power in different systems, and the SMN, DMN and VIS contributed the top predictive power (27.2%, 21.1%, and 15.1%, respectively). FED, first-episode; OA, onset age; HDRS, Hamilton depression rating scale.

Tables

Table 1. Demographic, clinical and imaging quality characteristics

Center	Group	Age, mean (SD), yr	Sex (M/F)	Education, mean (SD), yr	Duration of illness, mean (SD), yr	Medicated (Yes/No)	HDRS*, mean (SD)	Mean FD, mean (SD), mm
CMU, Shenyang	Controls (N=249)	27.24 (8.20)	103/146	14.85 (3.23)			1.10 (1.68)	0.11 (0.06)
	Patient (N=125)	27.91 (9.70)	39/86	12.15 (3.07)	1.65 (3.17)	49/76	21.44 (8.67)	0.11 (0.07)
	t or χ^2/*P*	0.70/0.484	3.33/0.068	7.72/<0.001			33.71/<0.001	1.07/0.286
CSU, Changsha	Controls (N=108)	32.31 (7.96)	62/46	11.84 (3.40)			0.62 (0.88)	0.13 (0.06)
	Patient (N=177)	36.28 (10.21)	77/100	10.16 (3.43)	2.52 (3.83)	N.A.	31.39 (7.82)	0.14 (0.07)
	t or χ^2/*P*	3.45/0.001	5.19/0.023	4.02/<0.001			36.52/<0.001	0.88/0.382
GCMU1, Guangzhou	Controls (N=34)	30.09 (10.88)	10/24	13.68 (3.07)				0.10 (0.03)
	Patient (N=34)	29.41 (8.27)	9/25	13.00 (3.44)	0.65 (0.70)	0/34	21.85 (2.25)	0.09 (0.03)
	t or χ^2/*P*	0.29/0.774	0.07/0.787	0.86/0.395				0.32/0.750
GCMU2, Guangzhou	Controls (N=66)	29.33 (10.12)	31/35	12.47 (2.53)				0.09 (0.04)
	Patient (N=66)	29.48 (9.91)	25/41	12.18 (3.09)	0.76 (1.00)	0/66	22.30 (3.57)	0.09 (0.06)
	t or χ^2/*P*	0.29/0.774	1.12/0.291	0.59/0.559				0.29/0.770
KMU, Kunming	Controls (N=50)	39.72 (11.97)	28/22	15.72 (3.88)				0.17 (0.06)
	Patient (N=41)	34.20 (9.37)	20/21	11.73 (4.35)	1.13 (1.28)	N.A.	23.61 (4.64)	0.19 (0.08)
	t or χ^2/*P*	2.47/0.015	0.47/0.492	4.62/<0.001				1.26/0.211
PKU, Beijing	Controls (N=73)	31.90 (9.01)	42/31	15.23 (2.28)				0.18 (0.07)
	Patient (N=75)	31.51 (7.86)	44/31	13.76 (3.02)	0.52 (0.47)	0/75	25.35 (4.77)	0.18 (0.06)
	t or χ^2/*P*	0.29/0.775	0.02/0.889	3.39/0.001				0.91/0.363
SCU, Chengdu	Controls (N=41)	34.83 (17.69)	17/24					0.12 (0.07)
	Patient (N=50)	34.44 (12.90)	25/25	16.08 (4.22)	1.17 (1.60)	25/25	22.88 (4.25)	0.11 (0.07)
	t or χ^2/*P*	0.12/0.904	0.66/0.416					0.71/0.479
SWU, Chongqing	Controls (N=254)	39.65 (15.80)	88/166	12.80 (4.25)				0.13 (0.06)
	Patient (N=282)	38.74 (13.65)	99/183	11.83 (3.72)	4.20 (5.52)	124/125	20.78 (5.88)	0.13 (0.05)
	t or χ^2/*P*	0.72/0.472	0.01/0.911	2.84/0.005				1.68/0.094
YMU, Taipei	Controls (N=109)	51.12 (11.70)	88/166	14.83 (3.64)				0.13 (0.06)
	Patient (N=105)	57.05 (16.21)	99/183	11.44 (4.36)	1.21 (1.54)	79/26	11.66 (6.99)	0.14 (0.08)
	t or χ^2/*P*	3.06/0.003	0.01/0.911	6.15/<0.001				1.17/0.243
ZZU, Zhengzhou	Controls (N=100)	22.43 (4.49)	47/53	15.02 (3.71)				0.09 (0.04)
	Patient (N=195)	18.40 (5.54)	97/98		1.28 (1.48)	0/195	22.43 (5.71)	0.10 (0.04)
	t or χ^2/*P*	6.29/<.001	0.20/0.655					2.16/0.032

Abbreviations: SD, standard deviation; M, male; F, female; HDRS, Hamilton depression rating scale; FD, framewise displacement; CMU, China Medical University; CSU, Central South University; GCMU, Guangzhou University of Chinese Medicine; KMU, Kunming Medical University; PKU, Peking University; SCU, Sichuan University; SWU, Southwest University; YMU, National Yang-Ming University; ZZU, Zhengzhou University; N.A., not available.

*The 17-item HDRS was used in the research centers of CMU, GCMU, KMU, PKU, SCU, SWU and ZZU. The 21-item HDRS was used in the research center of YMU. The 24-item HDRS was used in the research center of CSU.